ARL-TR-10325 ● APR 2026

Mechanical Response of Five Metals at Strain Rates Approaching 100 k/s

by Daniel Casem and Timothy Walter

NOTICES

Disclaimers

ARL-TR-10325 ● APR 2026

Mechanical Response of Five Metals at Strain Rates Approaching 100 k/s

Daniel Casem and Timothy Walter
DEVCOM Army Research Laboratory

REPORT DOCUMENTATION PAGE

1. REPORT DATE	2. REPORT TYPE	3. DATES COVERED START DATE	3. DATES COVERED END DATE
April 2026	Technical Report	10/1/2023	9/30/2025

4. TITLE AND SUBTITLE
Mechanical Response of Five Metals at Strain Rates Approaching 100 k/s

5a. CONTRACT NUMBER	5b. GRANT NUMBER	5c. PROGRAM ELEMENT NUMBER
5d. PROJECT NUMBER	**5e. TASK NUMBER**	**5f. WORK UNIT NUMBER**

6. AUTHOR(S)
Daniel Casem and Timothy Walter

7. PERFORMING ORGANIZATION NAME(S) AND ADDRESS(ES)	8. PERFORMING ORGANIZATION REPORT NUMBER
DEVCOM Army Research Laboratory ATTN: FCDD-RLA-TB Aberdeen Proving Ground, MD 21005	ARL-TR-10325

9. SPONSORING/MONITORING AGENCY NAME(S) AND ADDRESS(ES)	10. SPONSOR/MONITOR'S ACRONYM(S)	11. SPONSOR/MONITOR'S REPORT NUMBER(S)

12. DISTRIBUTION/AVAILABILITY STATEMENT
DISTRIBUTION STATEMENT A. Approved for public release: distribution unlimited.

13. SUPPLEMENTARY NOTES
ORCID: Daniel Casem, 0000-0002-0475-0226

14. ABSTRACT
Stress–strain curves were measured for five materials: 6061-T6511 aluminum, ETP copper, AZ31B-TP magnesium, 17-4 PH 900 stainless steel, and 702 zirconium. The experiments were all room-temperature uniaxial stress compression, using either a conventional load frame (strain rate of 0.0014/s) or a variety of miniature Hopkinson/pressure bar techniques (rates from 3000 to 100,000/s). A notable finding is that none of the materials exhibit a strong enhanced strain-rate sensitivity at the higher strain rates; the flow stresses for all materials increase linearly with the logarithm of strain rate over the ranges investigated. Vickers hardness measurements are also given for each material.

15. SUBJECT TERMS
mechanical behavior, high strain rate, miniature Kolsky bar, miniature split-Hopkinson pressure bar, enhanced strain rate sensitivity, Terminal Effects

16. SECURITY CLASSIFICATION OF: a. REPORT	b. ABSTRACT	C. THIS PAGE	17. LIMITATION OF ABSTRACT	18. NUMBER OF PAGES
UNCLASSIFIED	UNCLASSIFIED	UNCLASSIFIED	UU	26

19a. NAME OF RESPONSIBLE PERSON	19b. PHONE NUMBER *(Include area code)*
Timothy Walter	(520) 691-5411

STANDARD FORM 298 (REV. 5/2020)
Prescribed by ANSI Std. Z39.18

Contents

List of Figures

List of Tables

Acknowledgments

We would like to thank Dr. Daniel Field for conducting the XRF analysis of the stainless steel.

1. Introduction

The objective of this work is to measure the mechanical response of 6061-T6511 aluminum, electrolytic tough pitch (ETP) copper, AZ31B-TP magnesium, 17-4 PH 900 stainless steel, and 702 zirconium at strain rates from 0.0014 to 100,000/s. A major objective is to determine if there is an enhanced strain-rate sensitivity (SRS) at the high end of this range. Therefore, the bulk of the experiments are high-rate methods, either Kolsky bar (split-Hopkinson pressure bar)[1–4] or some modification thereof.

Typically, pressure bar methods are used to obtain strain rates from 1000 to 5000/s. However, miniaturized versions can be used to obtain higher rates,[5–13] and a good approach to achieve increasingly higher strain rates is to reduce bar diameter (along with sample size) until either the desired strain rate is obtained or practical difficulties prevent further miniaturization.[8,13] These are typically related to bar alignment, sample manufacture, or instrumentation. For this reason, three different pressure bar methods are used in this work. These methods are listed in Table 1 and described briefly in Section 2 and in more detail in the references.

Table 1. Methods used to obtain different strain rates.

Method	Strain rates (/s)	Nominal sample size (mm)
Servo hydraulic load frame	0.0014	1.5
3-mm-diameter Kolsky bar	3000–20,000	1.5
1.6-mm-diameter direct impact (DI)	10,000–40,000	0.7
0.8-mm flyer-loaded DI	20,000–100,000	0.350

Note: The three pressure bar methods overlap in strain rates so consistency between methods can be verified.

Any given pressure bar method is suitable for a fairly narrow range of strain rates, and the methods used here were chosen so that these ranges overlap to demonstrate consistency between them. In this report, stresses and strains are positive in compression.

2. Experimental Techniques

2.1 Sample Fabrication

All samples were cut from plate stock. All tests, including the Vickers hardness (HV) measurements, were performed so that the loads were applied in the plates' thickness directions, i.e., perpendicular to the faces of the plates. This includes the experiments on magnesium, which is highly anisotropic. All tests were at room temperature (294 K).

Three different sample sizes were used for the compression tests. All samples were nominally cubes with sizes of 1.5 mm, 0.7 mm, and 350 μm, and were cut from material from the interior of the plate, generally from the center half of the thickness dimension. The two larger sizes were made with electro-discharge machining (EDM), with the EDM finish removed by polishing to a 3-μm final finish. The smallest samples were made with a wire saw (Princeton Scientific WS22) using an 800-grit SiC abrasive slurry. These samples are difficult to polish after they are cut; as a result, the final samples have a 1–3 μm finish on the loading faces and the four lateral faces are as cut by the wire saw.

2.2 Low-Rate Experiments

Low-rate compression experiments (0.0014/s) were conducted with an Instron series 5984 hydraulic load frame. Sample load was measured with an Instron series 2580-10KN load cell. Sample compression was measured from the known crosshead motion using a correction for machine compliance. Loading faces were lubricated with Dow Corning Molykote 1122 grease. The 1.5-mm sample size was used for these experiments.

2.3 3-mm-diameter Kolsky Bar

A 3.18-mm-diameter Kolsky bar ("the 3-mm bar") was used to test the 1.5-mm samples at rates from 3000 to 20,000/s. The input bar was tool steel (Rockwell C hardness [RC] 60) and 406 mm long. Two output bars were used, depending on the experiment, both 3.18 mm in diameter. The first was tool steel and 229 mm long. The other was C2 tungsten carbide (WC) and 153 mm long. The use of the WC output bar has several advantages (i.e., more constant strain rates applied to the sample, improved accuracy of sample load as measured by the input bar, and less indention effect of the sample into the end of the bar), especially with the stronger materials. The input bar was instrumented with conventional strain gages at the midpoint in the standard fashion. The output bar was instrumented with a normal displacement interferometer (NDI) on the free end,[9,10] using a 150-mW, 532-nm laser (Coherent Sapphire SF-532-150 CW CDRH). Depending on the needs of the experiment, 3.18-mm-diameter steel strikers were used, either 51 or 142 mm long. Sample loading surfaces were lubricated with DuPont Molykote high-vacuum grease.

2.4 1.6-mm-diameter Direct Impact (DI)

A 1.6-mm-diameter DI method[14–17] was used to test the 0.7-mm samples at rates from 10,000 to 40,000/s. DI experiments typically use strain gages as instrumentation, but here the free end of the output bar is instrumented with an NDI, analogous to the methods described in Casem et al.,[9] to measure its velocity, v_f, directly. This is depicted in Figure 1.

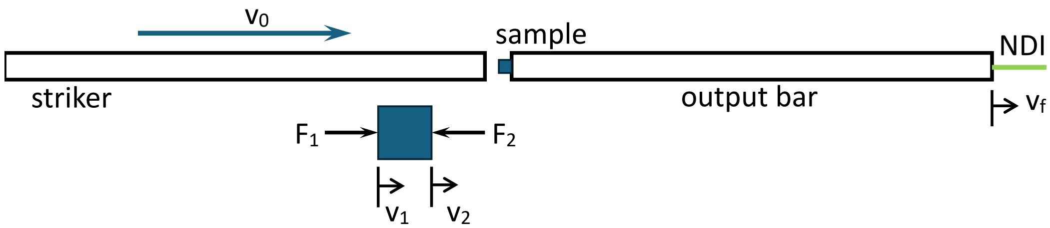

Figure 1. A symmetric DI method where the free end of the output bar is measured with an interferometer.

This instrumentation is somewhat novel; therefore, the analysis procedure is summarized as follows. The goal is to determine sample stress and strain from the NDI measurement. The output bar is initially stationary, with the sample adhered to one end with a thin layer of vacuum grease. The striker is launched from a gas gun at a known speed, v_0. Conditions are such that both the striker and the output bar remain elastic and the sample deforms plastically. Upon impact, the sample is compressed and it exerts force on both bars. The wave mechanics that result from this force on the output bar produce a free-end velocity, v_f, which is measured by the NDI. The force the sample applies to the output bar, F_2, and the velocity of that interface, v_2, can be found by an appropriate wave analysis.[9]

$$v_2(t) = \frac{1}{2}\left(v_f\left(t + \frac{L_o}{c_o}\right) + v_f\left(t - \frac{L_o}{c_o}\right)\right) \tag{1}$$

$$F_2(t) = \frac{A_o \rho_o c_o}{2}\left(v_f\left(t + \frac{L_o}{c_o}\right) - v_f\left(t - \frac{L_o}{c_o}\right)\right) \tag{2}$$

L_o is the length of the output bar, c_o is the bar wave speed, A_o is the area of the output bar, and ρ_o its density.

Upon impact, there is a brief non-equilibrium time in the sample that is assumed negligible.[18] Therefore, the sample is in a state of quasistatic equilibrium and

$$F_1 = F_2. \tag{3}$$

By symmetry, the motion of the interface between the sample and the striker bar can be found.

$$v_1(t) = v_0 - v_2(t) \tag{4}$$

This is valid provided the striker is in contact with the sample; effectively when F_2 is nonzero. Displacements of each end of the sample, u_1 and u_2, can be found by integrating v_1 and v_2. Specimen engineering strain and stress are then

$$\epsilon_s = \frac{u_1 - u_2}{L_s} \tag{5}$$

$$\sigma_s = \frac{F_2}{A_s} \tag{6}$$

One disadvantage of this method is the assumption that the sample is in equilibrium. If this is not the case, one could instrument the striker with an NDI on its free end so that F_1 and v_1 could be determined directly from that measured velocity in a manner identical to that done with the output bar. This instrumentation is somewhat more difficult to implement because of the need to instrument along the barrel of the gun and was not used here. Also, if the striker and output bar are dissimilar, a more complicated analysis is necessary where v_1 is determined from a 1D wave analysis of the striker in which the known force F_1 is applied to one end. However, this was not necessary for the experiments discussed herein.

2.5 0.8-mm-diameter Flyer-Loaded Direct Impact (FLDI)

The 350-µm samples were tested with FLDI. In this method, the traditional striker of the DI method is replaced with a large flyer plate. This avoids difficulties with alignment and instrumentation that arise as bar and sample sizes decrease, see Casem[19] for details. The output bar was 800-µm diameter and made from RC 60 tool steel, 28 mm long; samples were initially mounted with vacuum grease. The flyer was also tool steel (RC 60), 9.5 mm long and 9.2-mm diameter. Flyer speed was measured with a laser break and the output bar was instrumented with an NDI on the free end. Impact speeds ranged from 10 to 45 m/s to obtain rates from 20,000 to 100,000/s.

3. Results

This section presents the stress–strain curves for each material along with flow stress as a function of strain rate. The HV results are also presented. True stress and true strain are calculated assuming constant volume deformation. Compressive stress and strain are plotted as positive. All pressure bar data has been corrected for dispersion and the low-rate data has been corrected for machine compliance. The vertical scales for the flow stress versus rate plots do not start at zero stress so the scatter in the data can be seen more easily.

The rate effect plots give flow stress at a true stain of 0.1, along with a least squares logarithm fit to the data (linear on the semi-log plots). During any given experiment, strain rate is not necessarily constant; this is especially true for the high-rate experiments, although the stated values are good estimates. The low-rate data is largely isothermal and the high-rate is adiabatic.

3.1 6061-T6511 Aluminum

All samples of aluminum 6061-T6511 were machined from a single piece of nominally 6.35-mm-thick plate. Physical and mechanical properties are widely reported; typically, elastic modulus is 68–70 GPa, Poisson's ratio is 0.33, density is 2700 kg/m^3, and melting point about 858 K. Figure 2 shows the stress–strain curves for this material. Stress and rate at 10% true strain taken from these plots are plotted in Figure 3. Of all the materials discussed in this report, this one shows the strongest evidence for an enhanced SRS, which is easily seen by the deviation of the high-rate data from the least squares logarithmic fit shown on the graph. However, relative to the overall strength of the material, this deviation is small. None of these samples failed over the strain range plotted. This can be seen from the unloading curves that show elastic recovery. The data from each different method and sample size are plotted separately to show the consistency between the different datasets.

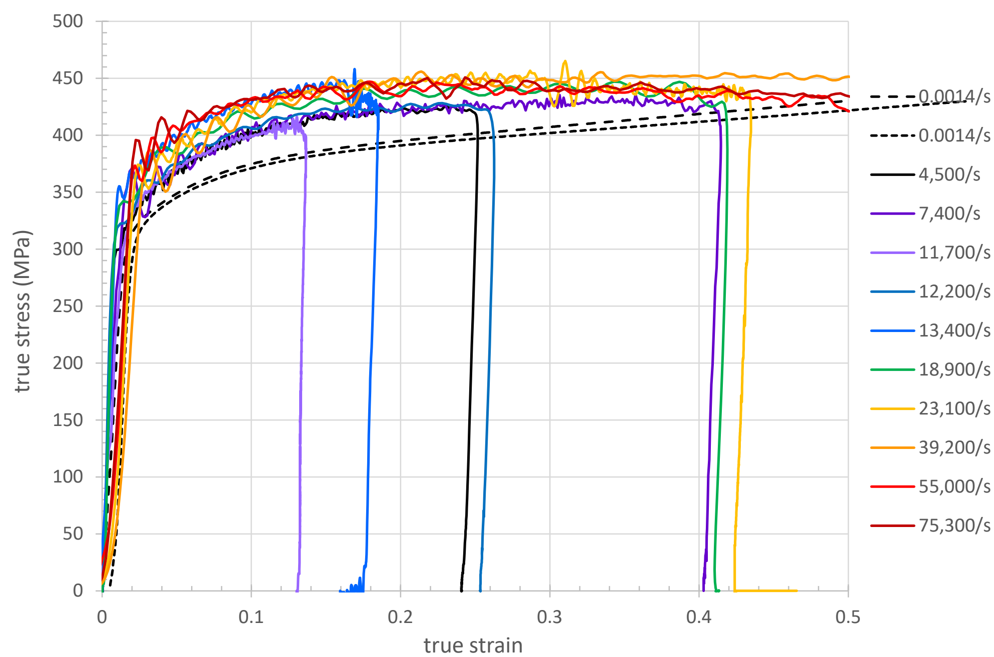

Figure 2. Stress–strain curves for aluminum 6061-T6511. The legend gives the instantaneous strain rate at 0.1 strain.

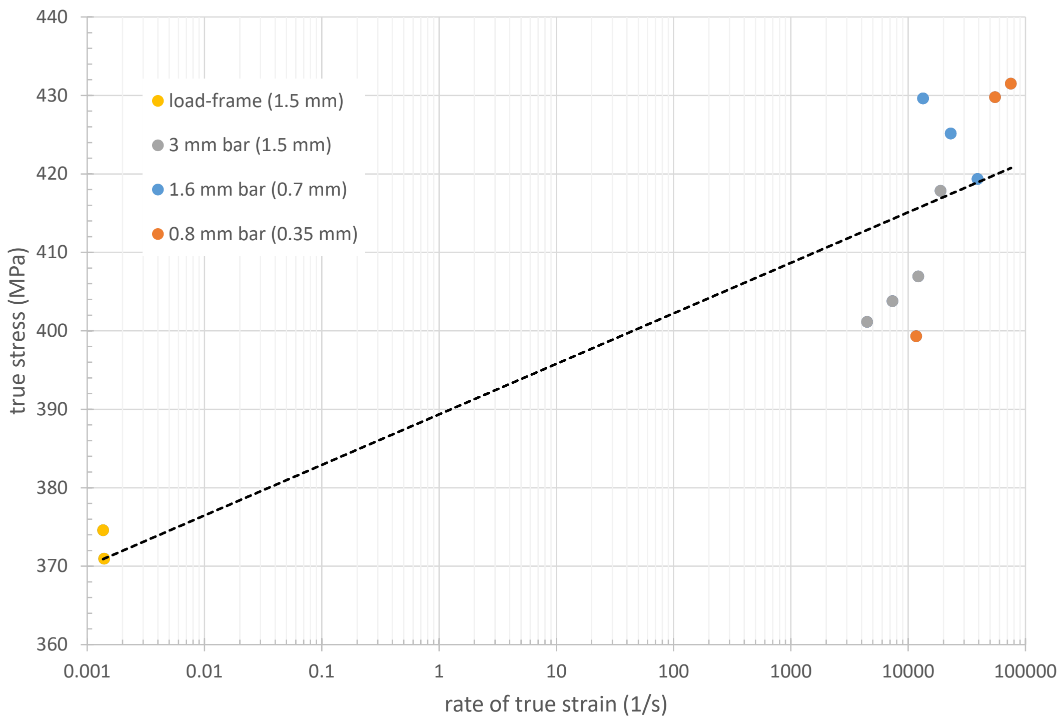

Figure 3. Rate effect for aluminum 6061-T6511. Values taken at 0.1 true strain.

3.2 ETP Copper

ETP copper is also known as 110 or C11000. The material tested here is annealed, with a Rockwell F hardness of 50.4. Basic physical and mechanical properties are widely available; elastic modulus of about 115–120 GPa, Poisson's ratio of 0.33, density of 8900 kg/m^3, and a melting point of 1356 K. All samples were machined from a nominally 6.35-mm-thick plate. The stress–strain curves are shown in Figure 4, and the stress at 10% strain versus rate is plotted in Figure 5. As seen for the aluminum alloy, none of these samples failed over the strain range plotted.

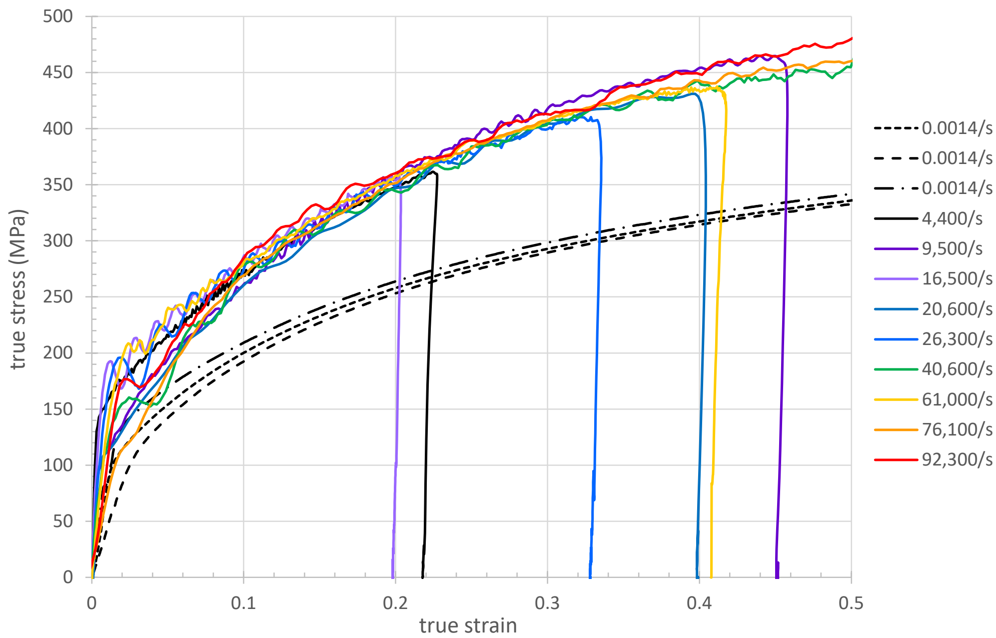

Figure 4. Stress–strain curves for ETP copper. Rates are given for the rate at 0.1 strain.

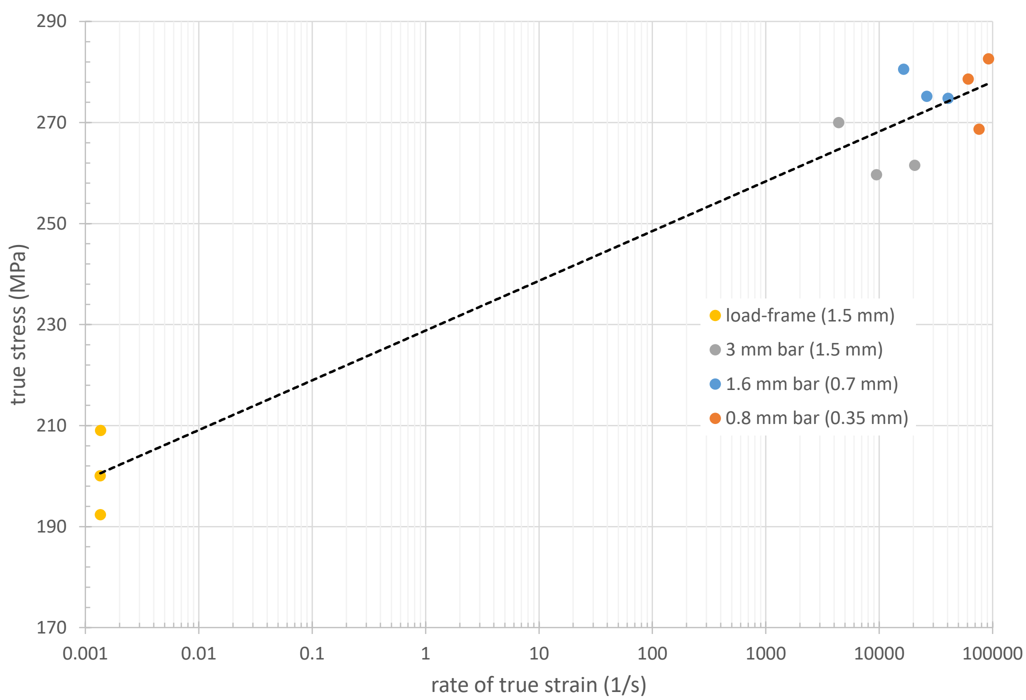

Figure 5. Rate effect for ETP copper. Values taken at 0.1 true strains.

3.3 AZ31B-TP Magnesium

AZ31B-TP is a wrought magnesium alloy that has been manufactured as tooling plate. It has a low density, typically reported at 1770 kg/m^3. Other typical reported properties are an elastic modulus of 45 GPa and a melting point of 880 K. It has hexagonal close-packed (hcp) crystal structure and is significantly anisotropic. In this work, it was only tested in the thickness direction of the plate, nominally 12.7 mm. The stress–strain curves are plotted in Figure 6. Most samples failed after each experiment; the recovered samples were in multiple pieces. The exceptions are the tests at 3,300 and 16,500/s, which show elastic unloading. In the other cases, it is unclear from the plots when the failure initiates, but it is reasonable to expect that the large stress drops after approximately 12% strain are due in part to some type of failure. Also note the large variation in behavior compared to the other materials.

Stress versus rate (at 10% strain) is plotted in Figure 7. In terms of the high-rate experiments, the data from the 0.7-mm samples (blue) show not only an increased scatter from the larger 1.5-mm samples (gray), but also a large decrease in strength. A similar inconsistency is seen with the smallest samples (350 µm; orange markers). This indicates a strong specimen size effect, indicating that the smaller sample sizes may not be representative of the continuum behavior and should be disregarded. For this reason, two least-squares logarithm fits are shown. The steeper slope omits the data from the two smallest sample sizes, and the other is a fit through all the data.

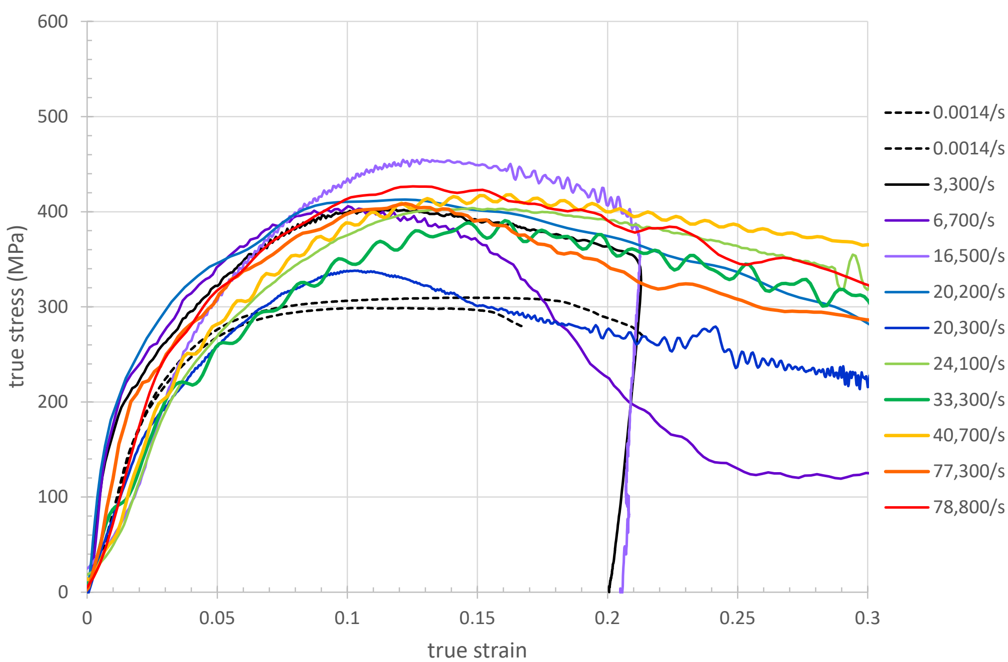

Figure 6. Stress–strain curves for AZ31B-TP magnesium. The rates are given at 0.1 strain.

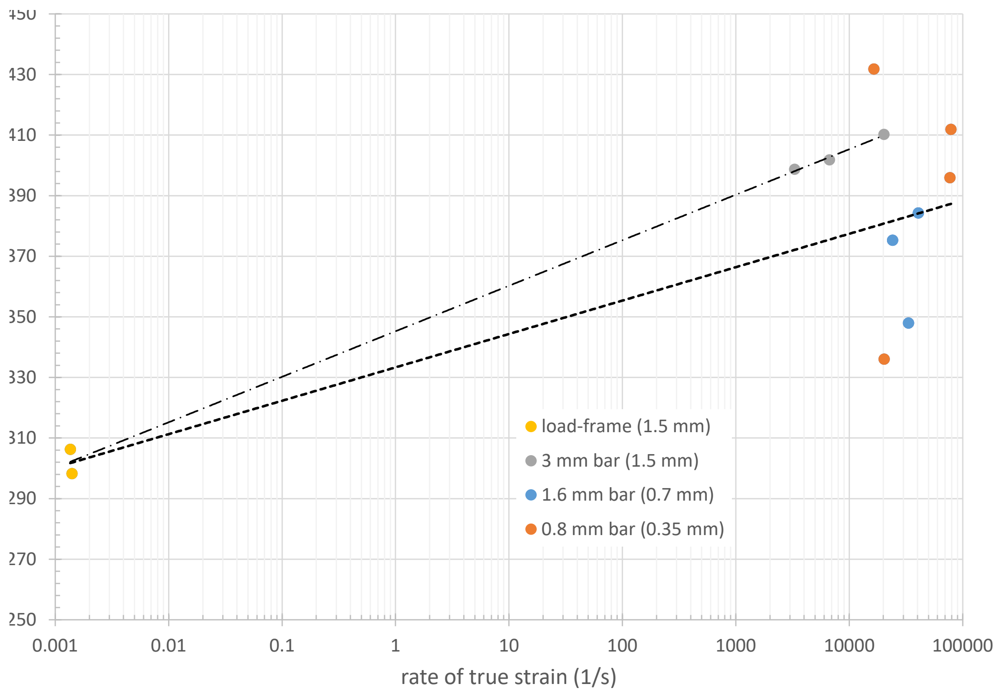

Figure 7. Rate effect for AZ31B-TP magnesium. Values are taken at 0.1 strain.

3.4 17-4 PH 900 Stainless Steel

Experiments were conducted on samples machined from 6.35-mm-thick 17-4 PH 900 stainless steel plate. An X-ray fluorescence (XRF) analysis produced the chemical composition in Table 2, which is out of bounds for the standard for 17-4, and closer to those for 15-5. The average HV measured for this material was 3888 MPa, which corresponds to a Rockwell hardness of RC 40.5 according to ASTM E140.[20] Typical reported properties include a density of approximately 8000 kg/m³, a melting point of 1670 K, and an elastic modulus of about 193 GPa. The stress–strain curves are presented in Figure 8 and the flow stress versus rate at 10% true strain is shown in Figure 9. None of these samples failed.

Table 2. Composition of the 17-4 PH 900 stainless steel measured by XRF.

Element	%	±
Fe	77.11	0.19
Cr	13.92	0.14
Ni	4.63	0.12
Cu	3.08	0.08
Mn	0.73	0.08
Nb	0.39	0.01
Mo	0.136	0.007

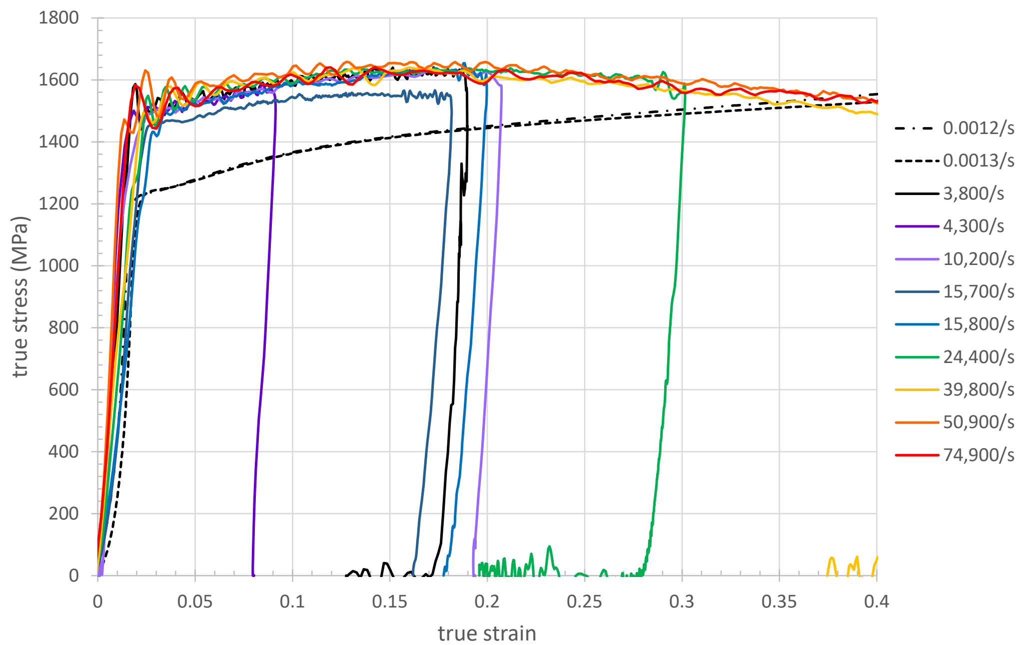

Figure 8. **Stress–strain curves for 17-4 PH 900 stainless steel. Rates are given at 0.1 strain.**

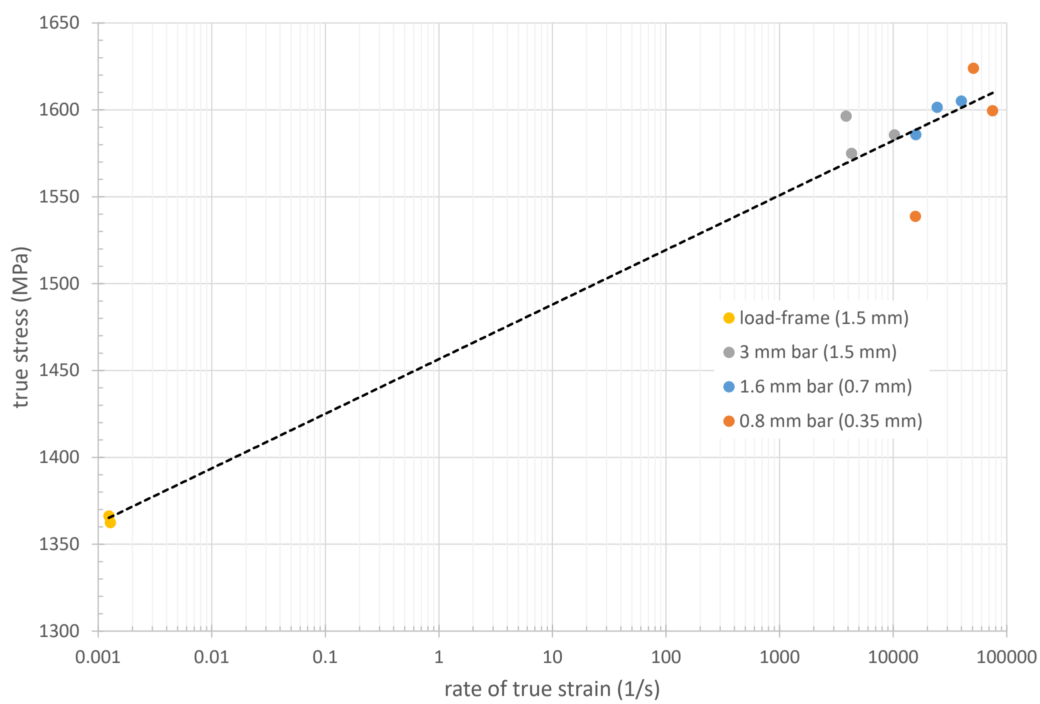

Figure 9. **Rate effect for 17-4 PH 900 stainless steel. Values are at 0.1 true strain.**

3.5 Zirconium 702

Zirconium 702 (Zr-702) is commercially pure. Typical reported properties include a density of approximately 6510 kg/m³, a melting temperature of 2125 K, and an elastic modulus of 99 GPa. The samples were cut from 3.18-mm plate. Like Mg, it is an hcp metal and when worked it can develop texture leading to anisotropy. It was only tested in the thickness direction.

Most of Zr-702 samples failed when tested at the higher strain rates. As suggested for Mg, it is unclear when failure initiates but the stress collapses that are evident beyond approximately 15% true strain are likely due in part to failure. Also, Zr-702 is known to form shear bands, which would be consistent with the present data.

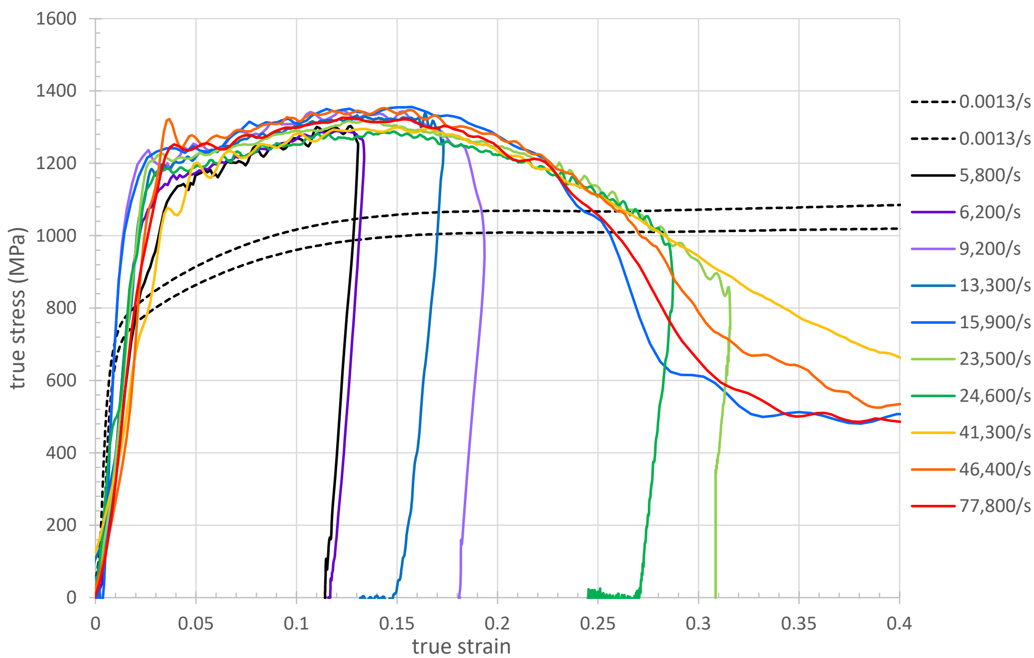

Figure 10. Stress–strain curves for Zr-702. Rates are given at 10% strain.

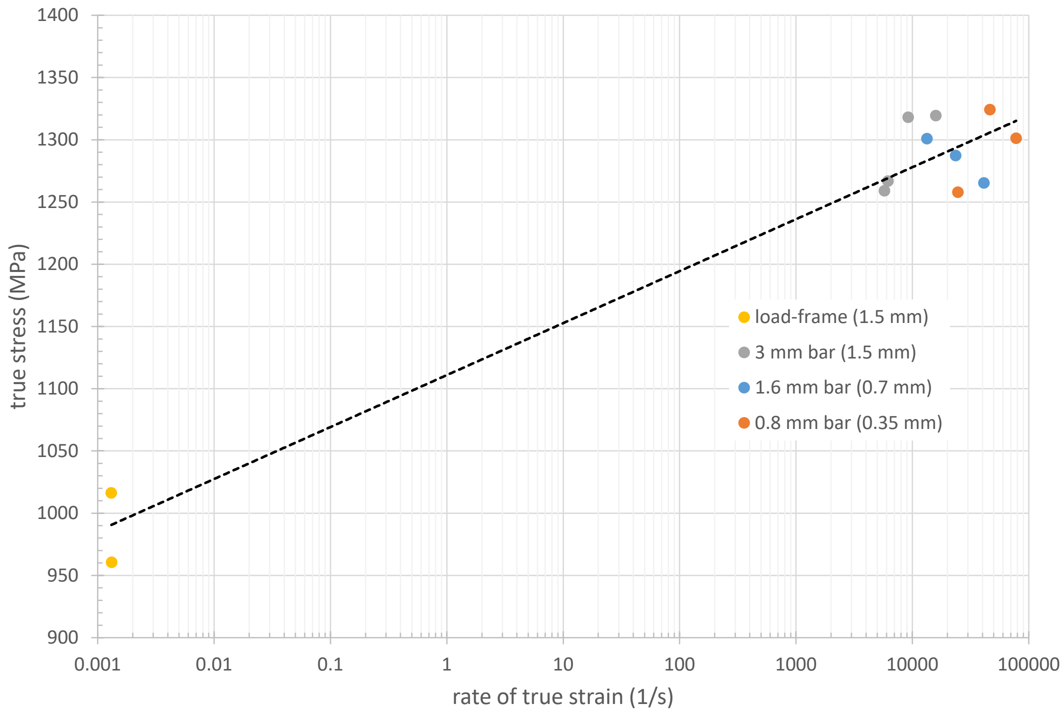

Figure 11. Rate effect for Zr-702 (values at 0.1 true strain).

3.6 Vickers Hardness (HV)

HV measurements were made with a Sun-Tech Corporation CM-400AT hardness tester, with 15-s hold times. Results for each material are given in Table 3 and Figure 12. This includes the length of each diagonal (D_1 and D_2), the average, and the calculated HV value for the corresponding load. In general, HV varies with load, although a systematic study of this variation was not performed. The average values given in the first column of Table 3 are averages of all hardness values for this material, regardless of the load.

Table 3. HV data for each material. All hardness tests were performed on planes parallel to the original faces of the plate.

Material	D_1 (µm)	D_2 (µm)	D_{ave} (µm)	Load (N)	Load (g-F)	HV (MPa)
6061-T6511 Al HV_{ave} = 1089 MPa	41.67	41.67	41.67	0.98	100	1047
	41.37	37.70	39.54	0.98	100	1163
	40.97	40.53	40.75	0.98	100	1095
	40.16	40.17	40.17	0.98	100	1127
	38.88	41.23	40.06	0.98	100	1133
	41.69	42.61	42.15	0.98	100	1024
	41.72	39.38	40.55	0.98	100	1106
	40.93	43.68	42.31	0.98	100	1016
ETP Cu HV_{ave} = 590 MPa	175.10	178.10	176.60	9.81	1000	583
	176.90	175.70	176.30	9.81	1000	585
	173.20	174.20	173.70	9.81	1000	603
AZ31B-TP Mg HV_{ave} = 564 MPa	180.90	178.70	179.80	9.81	1000	563
	178.30	181.50	179.90	9.81	1000	562
	182.50	175.70	179.10	9.81	1000	567
17-4 PH 900 stainless steel HV_{ave} = 3888 MPa	68.26	68.27	68.27	9.81	1000	3902
	68.47	68.89	68.68	9.81	1000	3855
	68.26	68.19	68.23	9.81	1000	3907
702-Zr HV_{ave} = 2001 MPa	32.40	30.48	31.44	0.98	100	1840
	30.49	29.39	29.94	0.98	100	2029
	29.95	30.50	30.23	0.98	100	1991
	40.16	42.36	41.26	1.96	200	2136
	43.06	41.99	42.53	1.96	200	2011
	42.37	42.88	42.63	1.96	200	2002

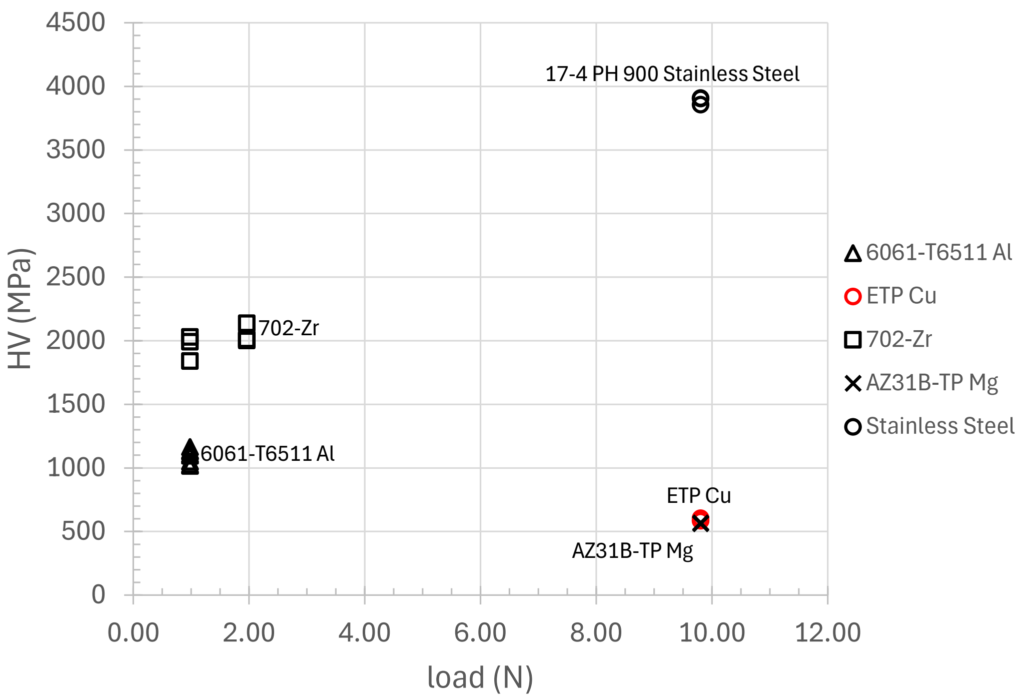

Figure 12. HV vs. applied load for each of the five metals.

4. Discussion and Conclusion

In summary, stress–strain curves are presented for a variety of metals, with specific emphasis placed on strain rates in the range of 10–100 k/s. This is the region where enhanced strain-rate sensitivity is often observed.[21] However, this is a difficult range to access experimentally, and the present work uses small-scale pressure bars as the overall approach. One drawback of this method is that it requires smaller and smaller samples to obtain higher and higher strain rates, which eventually leads to unacceptable errors due to sample fabrication and/or microstructural effects. This was not observed to be an issue for the materials tested here, with the exception of magnesium, and it is recommended to discount the data for this material using the two smallest sample sizes.

In terms of material behavior, a common concern is how to model the rate effect over the strain rates of interest. Many materials exhibit a linear relationship between flow stress and the logarithm of strain rate, as modelled by the Johnson–Cook strength model.[22] This approach seems adequate based on the data presented here. A possible exception to this is the aluminum alloy, but the deviation from linear behavior is slight and likely negligible for most applications. To emphasize this, the rate-hardening effects for each material are re-plotted in Figure 13 with an ordinate that begins at zero stress, making it easier to compare visually.

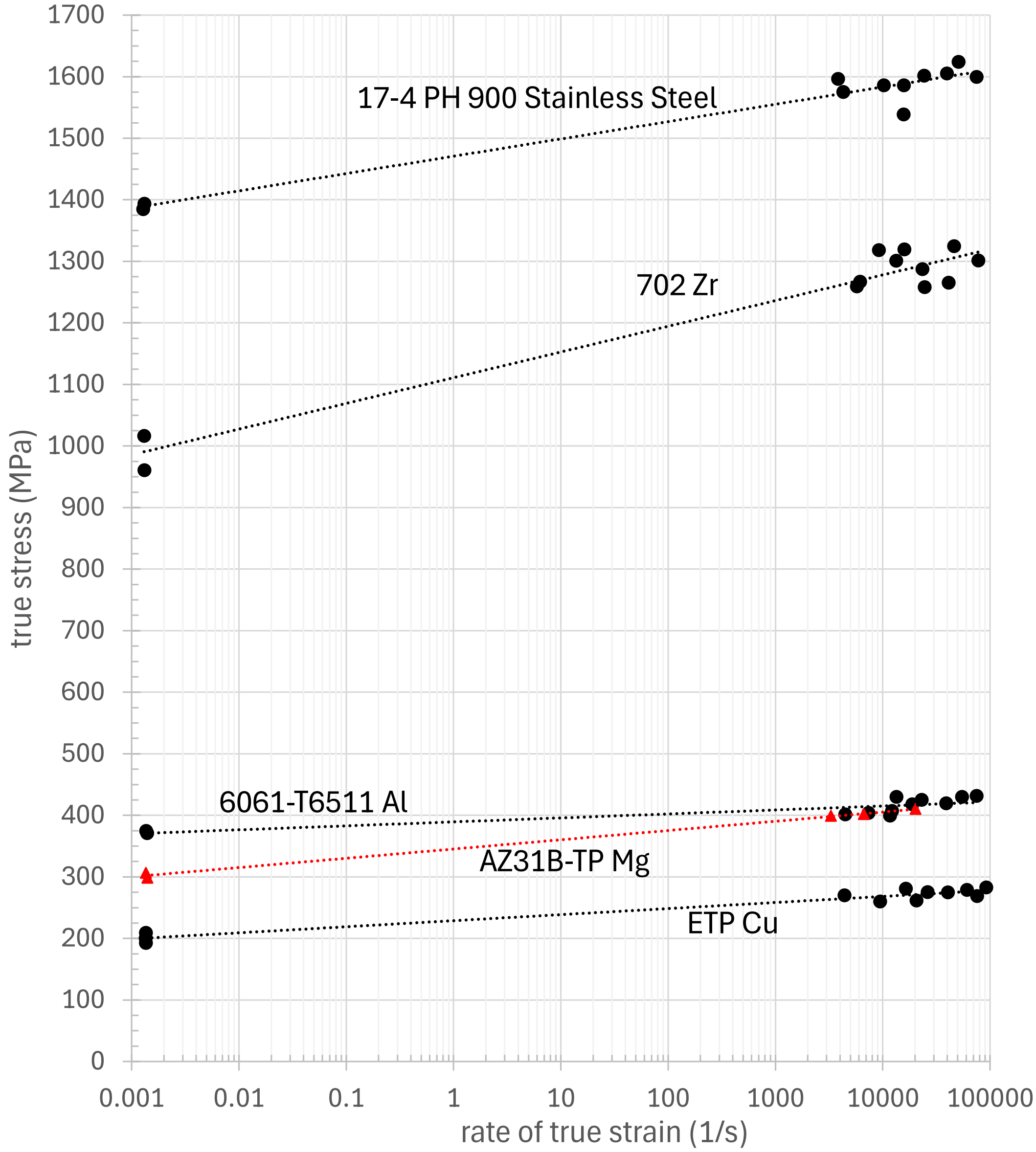

Figure 13. Rate effect for all materials. The magnesium data using 0.7- and 0.35-mm samples has been omitted due to the inconsistency with the larger samples.

In terms of future work, a more critical evaluation of the rate behavior could include additional repeats of the experiments described herein. However, a better approach might be to conduct additional experiments in the range accessible with load frames (0.01–1/s), and to attempt experiments at higher rates using the FLDI method using smaller sample sizes. It is reasonable to expect that rates as high as 500 k/s could be achieved using this method.

5. References

1. Kolsky H. An investigation of the mechanical properties of materials at very high rates of loading. Proc Phys Soc Lond B. 1949;62:676–700.
2. Follansbee PS. The Hopkinson bar. In: Metals handbook – ninth edition. (volume 8 – mechanical testing). American Society for Metals; 1985. p. 198–217.
3. Gray GT III. Classic split-Hopkinson pressure bar testing, In: Kuhn H, Medlin D, editors. Mechanical testing and evaluation, vol. 8. ASM International; 2002. p. 462–476.
4. Chen W, Song B. Split Hopkinson (Kolsky) bar. Mechanical Engineering Series. Springer; 2011.
5. Safford NA. Materials testing up to 10^5/s using a miniaturized Hopkinson bar with dispersion corrections. In: Zhemin Z, editor. Proceedings of the Second International Symposium on Intense Dynamic Loading and its Effects; 1992; Chengdu, Sichuan, China. Sichuan University Press; 1992. p. 378.
6. Kamler F, Niessen P, Pick RJ. Measurement of the behavior of high purity copper at very high rates of strain. Can J Phys. 1995;7:295–303.
7. Malinowski JZ, Klepaczko JR, Kowalewski ZL. Miniaturized compression test at very high strain rates by direct impact. Exp Mech. 2007;47:451–463.
8. Casem DT. A small diameter Kolsky bar for high-rate compression. Proceedings of the 2009 SEM Annual Conference and Exposition on Experimental and Applied Mechanics; 2009 June 1–4; Albuquerque, NM.
9. Casem DT, Grunschel SE, Schuster BE, Interferometric measurement techniques for small diameter Kolsky bars. Proceedings of the 2010 SEM Annual Conference and Exposition on Experimental and Applied Mechanics; 2010; Indianapolis, IN. p. 973–977.
10. Casem DT, Grunschel SE, Schuster BE. Normal and transverse displacement interferometers applied to small diameter Kolsky bars. Exp Mech. 2012;52(2):173–184.
11. Jia D, Ramesh KT. A rigorous assessment of the benefits of miniaturization in the Kolsky bar system. Exp Mech. 2004;44:445–454.
12. Heuzé T, Guo X, Othman R. Very high strain rate range. In: Othman R, editor. The Kolsky–Hopkinson bar machine. Springer; 2018. p. 249–272.

13. Casem D. Miniature Kolsky bar methods. Advances in experimental impact mechanics. Elsevier; 2022. p. 149–189.

14. Gorham DA, Pope PH, Field JE. An improved method for compressive stress–strain measurements at very high strain rates. Proc R Soc Lond A. 1992;438:153–170.

15. Couque H. The use of the direct impact Hopkinson pressure bar technique to describe thermally activated and viscous regimes of metallic materials. Phil Trans R Soc A. 2014;372.

16. Gorham DA. Measurements of stress–strain properties of strong metals at very high rates of strain. In: Harding J, editor. Proceedings of the Second Conference on Mechanical Properties of Materials at High Rates of Strain. Institute of Physics Conference Series no. 47; 1979 Mar 28–30; Oxford, England. p. 16–24.

17. Lea LJ, Jardine AP. Application of photon Doppler velocimetry to direct impact Hopkinson pressure bar. Rev Sci Instrum. 2016;87:023101.

18. Davies EDH, Hunter SC. The dynamic compression testing of solids by the method of the split Hopkinson pressure bar. J Mech Phys Solids. 1963;11(3):155–179.

19. Casem D. A flyer-loaded direct impact method for high strain-rate testing. J Dyn Behav Mater. Forthcoming 2026.

20. ASTM E140. Standard hardness conversion tables for metals relationship among Brinell hardness, Vickers hardness, Rockwell hardness, superficial hardness, Knoop hardness, Scleroscope hardness, and Leeb hardness. ASTM International; 2019 May.

21. Rosenberg Z, Kositski R, Ashuach Y, Leus V, Malka-Markovitz A. On the upturn phenomenon in the strength vs. strain-rate relations of metals. Int J Solids Struct. 2019;176–177:185–190.

22. Johnson GR, Cook WH. A constitutive model and data for metals subjected to large strains, high strain rates, and high temperatures. Proceedings of the 7th International Symposium on Ballistics; 1983 Apr 19–21; The Hague, the Netherlands.

List of Symbols, Abbreviations, and Acronyms

1D	One-Dimensional
ASTM	American Society for Testing and Materials
DI	Direct Impact
EDM	Electro-Discharge Machining
ETP	Electrolytic Tough Pitch
FLDI	Flyer-Loaded Direct Impact
hcp	Hexagonal Close Packed
HV	Vickers Hardness
NDI	Normal Displacement Interferometer
RC	Rockwell C Hardness
SRS	Strain-Rate Sensitivity
WC	Tungsten Carbide
XRF	X-Ray Fluorescence

1 (PDF)	DEFENSE TECHNICAL INFORMATION CTR DTIC OCA
1 (PDF)	DEVCOM ARL FCDD RLB CB TECH LIB